I. AAS 06-0XX

Numerical Skip-Entry Guidance

Michael Tigges
NASA/JSC

Timothy Crull
Jacobs Technology

Jeremy Rea
NASA/JSC

Dr. Wyatt Johnson
NASA/NSC

29th ANNUAL AAS GUIDANCE AND CONTROL CONFERENCE

February 4-8, 2006
Breckenridge, Colorado

Sponsored by
Rocky Mountain Section

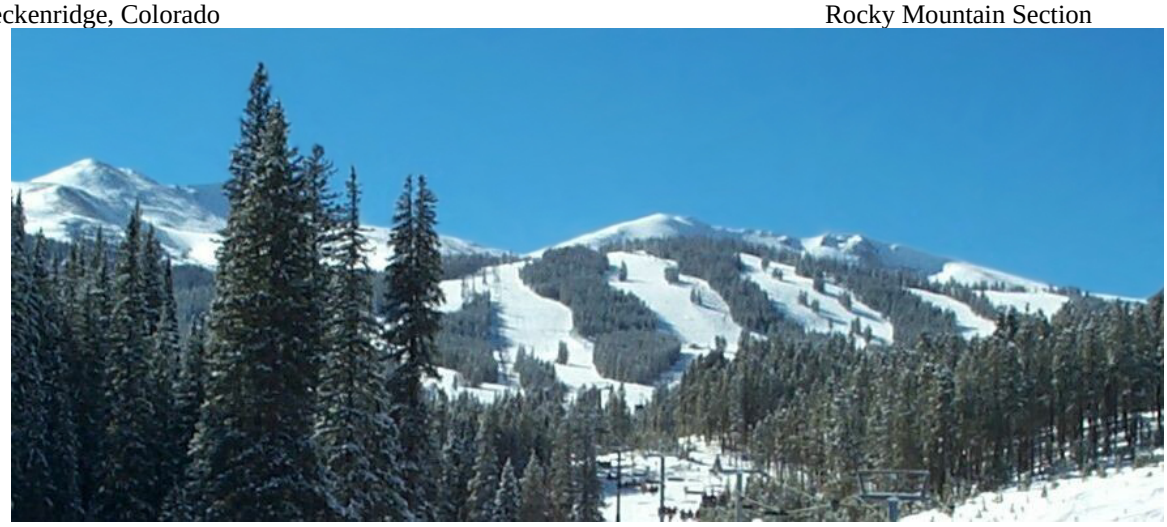

AAS Publications Office, P.O. Box 28130 - San Diego, California 92198

Numerical Skip-Entry Guidance

Michael A. Tigges* Timothy Crull† Jeremy Rea‡ Dr. Wyatt Johnson§
NASA Johnson Space Center, Houston, Texas, 77058

This paper assesses a preliminary guidance and targeting strategy for accomplishing Skip-Entry (SE) flight during a lunar return-capsule entry flight. One of the primary benefits of flying a SE trajectory is to provide the crew with continuous Continental United States (CONUS) landing site access throughout the lunar month. Without a SE capability, the capsule must land either in water or at one of several distributed land sites in the Southern Hemisphere for a significant portion of a lunar month using a landing and recovery scenario similar to that employed during the Apollo program. With a SE trajectory, the capsule can land either in water at a site in proximity to CONUS or at one of several distributed landing sites within CONUS, thereby simplifying the operational requirements for crew retrieval and vehicle recovery, and possibly enabling a high degree of vehicle reusability. Note that a SE capability does not require that the vehicle land on land. A SE capability enables a longer-range flight than a direct-entry flight, which permits the vehicle to land at a much greater distance from the Entry Interface (EI) point. This does not exclude using this approach to push the landing point to a water location in proximity of CONUS and utilizing water or airborne recovery forces.

Nomenclature

ARES = *Architecture for Exploration Studies*
Azimuth = *Measure of vehicle direction. 0º azimuth is due north*
AEG = *Apollo Entry Guidance*
CEV = *Crew Exploration Vehicle*
CM = *Crew Module*
Co-azimuth = *Complement of the azimuth angle (90º-azimuth). 0º is due east*
CRANGA = *Crossrange Error*
EI = *Entry Interface (400,000. ft, 121.92 km)*
GN&C = *Guidance Navigation and Control*
GRAM = *Global Reference Atmosphere Model*
I-Load = *Initialization load parameter*
ISS = *International Space Station*
KSC = *Kennedy Space Center*
L/D = *Lift-to-Drag ratio*
MC_OPS = *Monte Carlo Operational Data Sets*
NSEG = *Numeric Skip-Entry Guidance*
PET = *Phase Elapsed Time*
RCS = *Reaction Control System*
SE = *Skip Entry*
SM = *Service Module*
SORT = *Simulation and Optimization of Rocket Trajectories*
TEI = *Trans-Earth Injection maneuver*

*Senior Aerospace Engineer, Flight Mechanics & Trajectory Design Branch, Johnson Space Center, Houston, Tx.
†Senior Guidance Design Engineer, Jacobs Technology, Johnson Space Center, Houston, Tx.
‡Aerospace Engineer, Flight Mechanics & Trajectory Design Branch, Johnson Space Center, Houston, Tx.
§Aerospace Engineer, Flight Mechanics & Trajectory Design Branch, Johnson Space Center, Houston, Tx.

I. Introduction

A capsule vehicle in the 0.3–0.4 Lift-to-Drag (L/D) class returning from the Moon can fly a maximum of about 2000 nautical miles (nmi) range and 60 nmi crossrange using an Apollo-like direct entry. To fly longer range and/or crossrange, the capsule trajectory must be lofted to decrease aerodynamic forces. Lofting, or Up-Control, implies using the vehicle lift to push the vehicle out of the atmosphere and slow the rate at which energy is dissipated. During this high altitude low drag skip phase of the entry, the vehicle can dramatically increase the range and crossrange capability. In this report, a SE trajectory will be defined whenever the Up-Control drag acceleration drops below a threshold of about 6 fpss (0.2 Gs) during the Up-Control phase of flight. The crew flying on such a trajectory will experience a short exo-atmospheric phase of flight before the second entry.

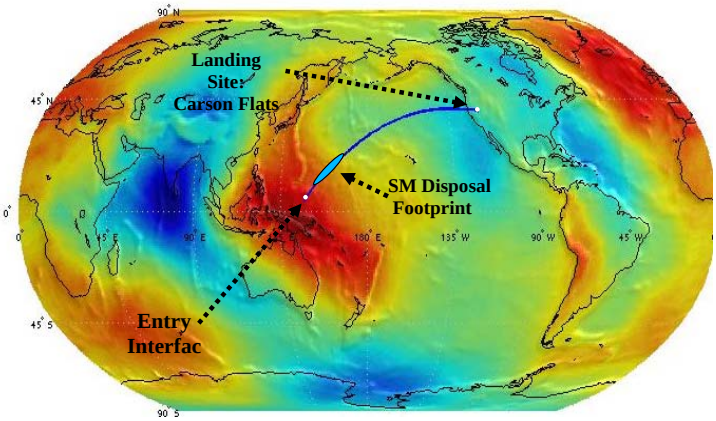

Figure 1. Skip-Entry Groundtrack. *Shown is a typical Skip-Entry groundtrack ascending right approach to Carson Flats, Nv, 5,400 nm flight range flight.*

The SE trajectory places the footprint for the SM far from the landing point (see Figure 1). By properly targeting the TEI maneuver at the Moon, the SM footprint can be safely disposed in water in an area close to the antipode of the lunar approach orbit. The antipode is a vector that points from the moon to earth at the time of lunar departure. A SE trajectory enables Crew Module (CM) landing anywhere within CONUS. In this report, however, only landing sites that are compatible with an International Space Station (ISS) return-entry flight will be considered. This will isolate landing sites to the Western CONUS.

Shown in figure 2 are the SE groundtracks and event sequences for four of the EI Operational Sites (OS1-4) under analysis in this report. Each of these four OS sites initializes an SE trajectory to Edwards Air Force Base (EAFB), California; and will be discussed in more detail in section II. The simulation starts at EI (EI = 400,000 feet, 121.92 km), with the vehicle postured in the middle of the SE flight corridor. The SE flight corridor is designed to maximize success for a nominal flight and to insure the safe abort landing of the crew in the event of a failure before EI that would require a downmode to a ballistic entry to the water (see Section III, SE Flight Corridor – Ballistic Entry). The nominal flight continues through the skip maneuver, coasts up to apogee, and then enters the atmosphere a second time and flies until drogue chute deployment in proximity of the targeted landing site. As shown, the flight time from EI to drogue

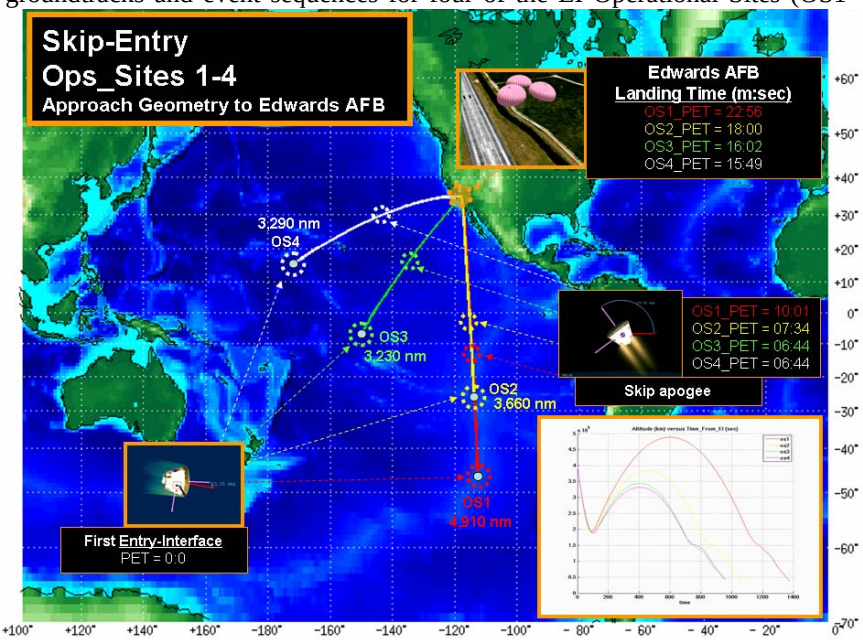

Figure 2. Entry Footprint. *Shown are four proposed Operational Test Sites under study in this report. Each site (OS 1-4) identifies the EI state consistent with access to a given landing site (Edwards AFB example shown).*

deployment can vary between 16 and 23 minutes for the flights under consideration. A large variability in the maximum altitude for the different ranges flown during the skip is also evident in this Figure.

II. Lunar Return Geometry

Several key components of the lunar return geometry as related to the landing footprint are presented. Figure 3 displays the groundtrack, antipode, Entry Interface (EI), and landing site for a 7,300 nm trajectory to KSC, Fla. Entry Interface is defined when the vehicle achieves 121.92 km (400,000 ft) altitude on the approach ellipse and the antipode defines a vector connecting the moon through the earth's center at time of lunar departure. The antipode moves from a maximum latitude point to a minimum latitude point and back again during each lunar month (~27.32 days). The extreme latitude for this movement ranges from ±28.6 degrees when the moon is at maximum inclination to ±18.3 degrees when the moon is at minimum inclination. The period for this motion is approximately 18.6 years.[5]

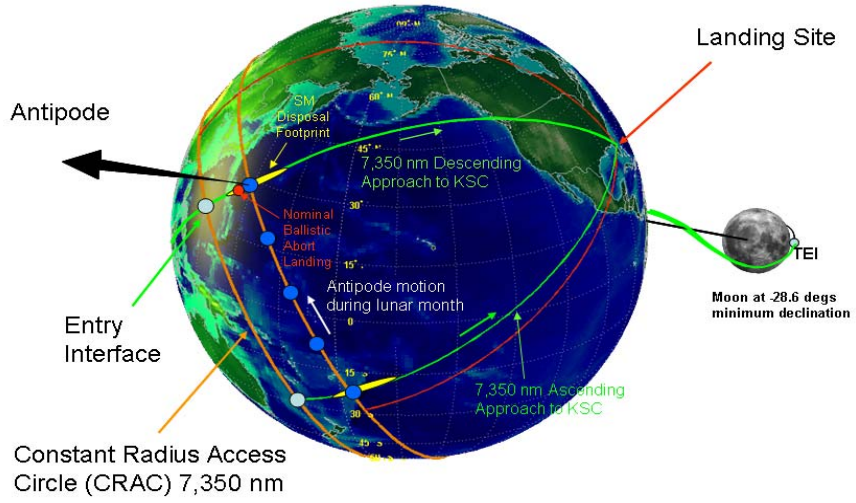

Figure 3. Entry Footprint. *Shown is the Earth-Moon geometry and Skip-Entry trajectory components for a 7,300 nm trajectory to KSC, Fla.*

Figure 4 shows how the antipode relates to EI, the vacuum perigee point, and the landing footprint for both lunar return Apollo direct entry and SE flight. The antipode is an important component of the entry design landing footprint since, for a lunar return direct entry, it is tied to and in proximity of the nominal landing site latitude. As shown, the landing footprint is much farther downrange for the SE. Note that EI, vacuum perigee, and the footprint are all tied together via the entry design process. The vehicle can land anywhere within the landing footprint using nominal lift-vector control. The longitude of the landing site is positioned within the entry footprint by varying the lunar trip time ±12 hours to allow the Earth to spin into the correct orientation; however, the location of vacuum perigee, and therefore the entry interface point and entry footprint, changes for different flight times. This shift is relative to the antipode, and along the groundtrack, and can be as large as 420 km (220 nmi) for a 3.5- to 4.5-day flight time variation direct entry scenario. Since the amount of flight-time longitude adjustment is not known until the time of lunar departure, the heel of the landing footprint must be designed worst-case to occur before the landing site/antipode. This design bias effectively reduces the 750-nmi Apollo direct entry footprint to approximately 520 nmi as shown.

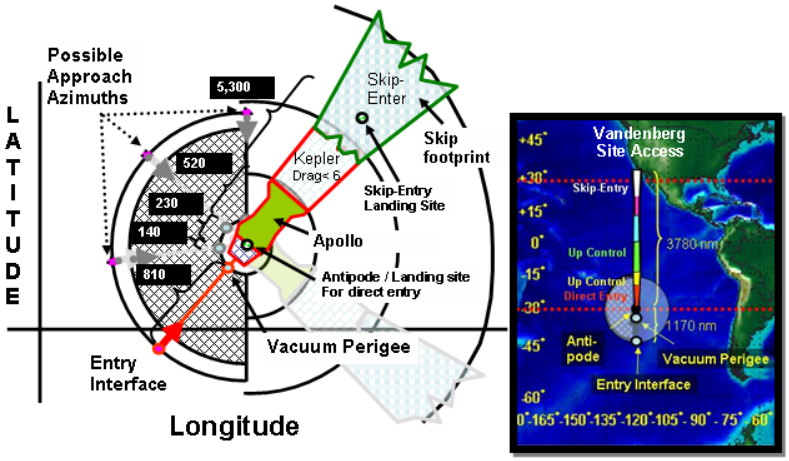

Figure 4. Entry Footprint. *Shown are the components of the entry footprint for a typical Apollo direct entry and 5,300 nm SE trajectories.*

Note also that the vacuum perigee point approximates the toe of the service module ballistic footprint. Service module disposal is an important consideration when designing the lunar return trajectory for vehicles that separate from a service module stage, since safe disposal of the surviving fragments is mandatory. Since the opening of the landing footprint for the SE flight occurs at a much greater distance downrange from the antipode, an entirely different geometry for the location of the service module disposal footprint is provided.

Finally, the approach direction (azimuth) of the entry groundtrack can be controlled via the lunar TEI maneuver for a cost of ~130 m/s, providing ±90º of co-azimuth control.[5] This delta-velocity permits rotation of the entry footprint about the departure antipode as depicted in Fig. 4 and enables an extra degree of freedom for controlling entry geometry and service module disposal for direct entry or SE flight trajectories.

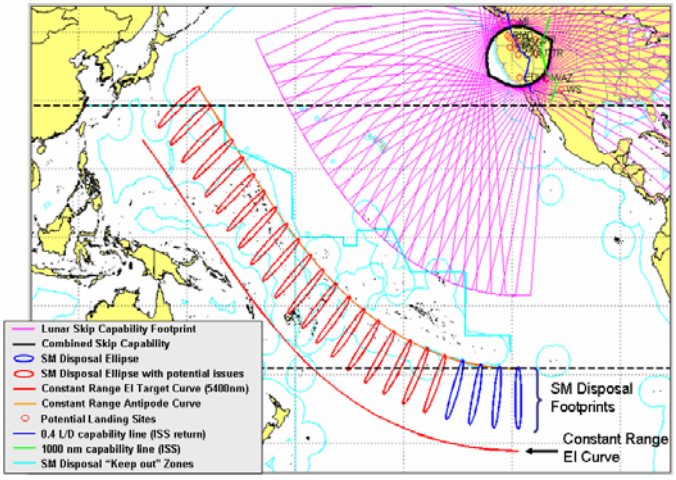

Figure 5. Skip-Entry Footprint Overlay. *Lunar skip capability footprint overlay with territorial water constraints.*

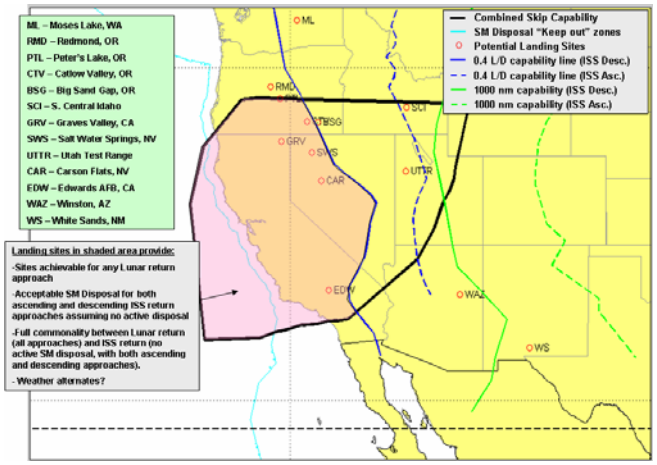

Figure 6. Entry Footprint. *Shown are the complementary ISS direct entry and SE CONUS landing sites created from the overlapping SE footprints from Section V.*

Figure 5 shows that, in the absence of SM disposal constraints, the arc of a constant range-to-target circle can be drawn throughout the lunar month that connects the EI point, the antipode, and a desired landing site. The nominal footprint of section V was superimposed for each flight on this figure. Standardizing the SE range would be a desirable goal for flight qualification reasons; however other constraints, most notably SM disposal, play an important role in dictating the allowed geometry for Skip-Return. Noteworthy on Figure 6, is an "eye" of possible primary and alternate CONUS landing sites defined throughout the lunar month. This eye is created by overlaying the guidance footprints introduced in Section V on the approach geometries across the month. The common area of intersection creates the eye. It will be possible to select a primary landing site within this eye and have confidence that an alternate landing site can be chosen late in the approach trajectory that will be within the footprint of the SE guidance.

Figure 6 shows a magnified view of the landing site eye. Recall that all landing sites within the eye are within the footprint capability of the SE guidance. Contained within Figure 6 are the landing sites under consideration in this report. Choosing a primary and alternate site(s) will depend on

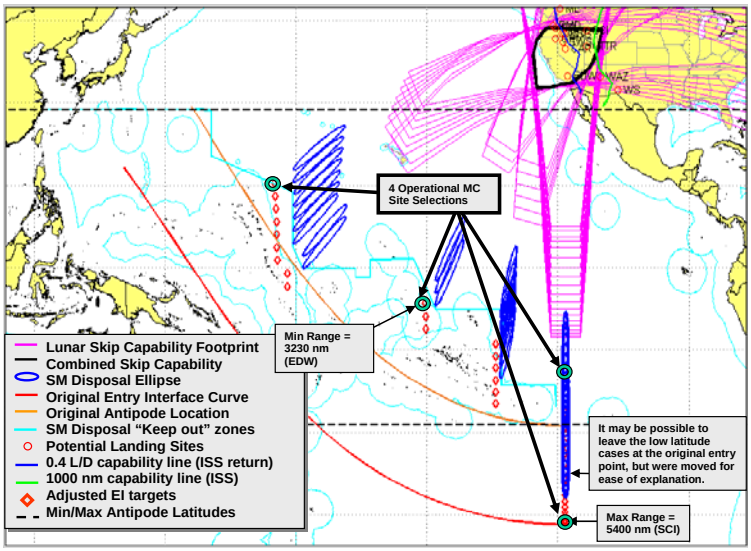

Figure 7. Entry Footprint. *Monte Carlo operational set definition (MC OPS1-4).*

many factors to ensure the availability of a given set under a wide range of possible conditions (e.g., weather, wind, facilities).

Figure 7 depicts a possible solution for moving the TEI targeted EI state throughout the lunar month that avoids territorial waters for SM disposal. In this report, four sets of operational sites are analyzed (drawn as green circles in the figure). A primary and alternate site was chosen (Table 1, section VI), and the performance of the SE guidance algorithm for accessing these sites was generated (Section VI).

III. Skip-Entry Flight Corridor

The SE flight corridor provides the appropriate flightpath angle at EI that enables satisfying all mission, crew, vehicle, and trajectory design considerations. These factors include acceleration magnitudes and durations, SM disposal, heat rate and heat load constraints, landing site precision, and safe landing after a failed GN&C.

Figure 8 provides bank-angle plots for the Numeric Skip-Entry Guidance (NSEG) guided SE flightpath-angle corridor. These flights were completed for a 4,910 nmi SE flight to EAFB. Note that the SE bank angle tends to lift-down as the overshoot side of the SE flightpath-angle corridor is approached; and tends to lift-up as the undershoot side of the SE flightpath-angle corridor is approached. This reduces the available margins for correcting the in-flight dispersions. These corridor extremes would never be flown for a nominal flight design, but act as boundaries for the SE corridor.

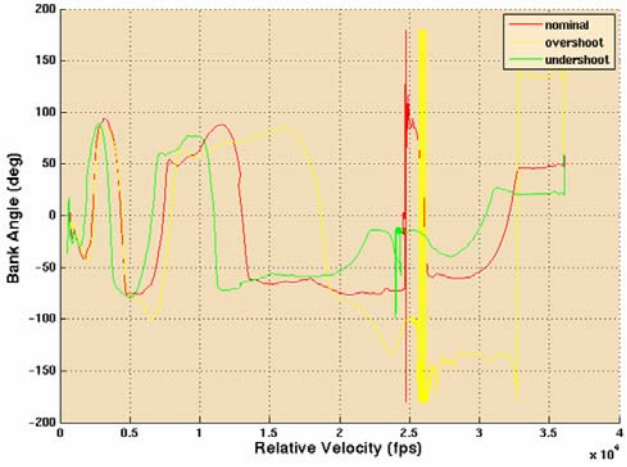

Figure 8. Guided (NSEG) SE Flight Corridor Bank Angles: *Shown are the nominal, overshoot, and undershoot trajectories for the SE flight corridor.*

Figure 9 constructs the Guided flyable flightpath-angle corridor in terms of flightpath-angle corridor "knockdowns" reserved for aerodynamic, atmosphere, and mass properties.[17] Under the assumption that these "knockdowns" are applicable to the SE problem, one obtains a flyable SE corridor of 1.25 degrees. As will be discussed, for this report the nominal EI flightpath angle was chosen on the steep side of the SE corridor to protect against crew module skip in the event of a ballistic entry downmode. A shallower flightpath angle is possible and perhaps desirable in terms of skip phase bank margins, but was not assessed in this analysis.

As shown in Figure 9, the overshoot corridor is flown at a deterministic maximum flightpath angle of -6.6 degrees, enabling successful SE landing with a peak skip G-load of 9 Gs. The undershoot side of the corridor is flown at a deterministic minimum flightpath angle of -4.8 degrees that enables precision landing at EAFB. These flightpath-angle values define the flightpath-angle corridor extremes for SE precision landing. A decision must now be made on what value to use for the nominal EI flightpath angle. From the corridor plot Figure 6, if precision landing is the only driving consideration, a nominal EI flightpath angle can be chosen anywhere within the range of -5.05 to -6.3 degrees.

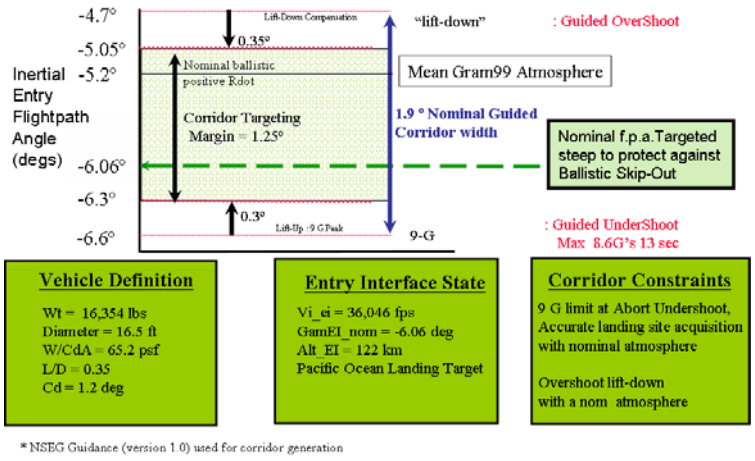

Figure 9. NSEG Precision Guided Flight Corridor *Shown is the available flightpath angle corridor for Skip-Entry design.*

However, the ballistic entry flight downmode requirement must be factored into the corridor design. Two factors that must be considered are skip-out and excessive G-

loads. Too shallow of a nominal EI flightpath angle and the probability for CM skip-out following ballistic downmode is increased. Too steep of a nominal EI flightpath angle and the probability for excessive crew acceleration after ballistic downmode is increased.

Two extreme flights shown in Figure 10 are useful for bounding the nominal EI flightpath. Both are generated with nominal simulation ballistic downmode conditions. A parametric scan of initial flightpath angles was performed until a nominal ballistic flight showed positive altitude rate during entry. Another steeper flight was generated that provided nominal accelerations of 18 Gs. These values were found to be -5.2 degrees for the positive altitude rate ballistic flight and -6.5 degrees for the 18-G nominal ballistic flight. Using these values as guidelines superimposed on the guided SE corridor of Figure 6, a selection for the nominal entry flightpath angle can be tentatively made. Conservatively, a value of -6.06 degrees will be assessed for the nominal flightpath. This is biased intentionally steep to stay away from the possibility of ballistic downmode skip-out. Recent analysis is indicating potential advantages for using shallower EI flightpath angles (e.g., -5.85 degs) to capture additional bank margins during the skip phase of flight; but this value will probably only be used if vehicle L/D drops lower than the current 0.35 value.

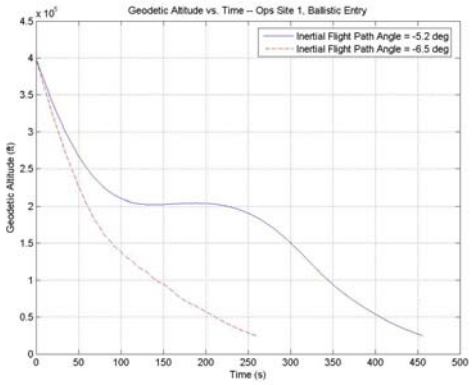

Figure 10. Ballistic Flight Boundar Flights *Shown are the guided peak acceleration and positive altitude rate (skip-out) bounding flights.*

IV. Numerical Skip-Entry Guidance (NSEG) Description

A number of different approaches to SE guidance have been under evaluation. Currently, a numerical approach, that uses multiple trajectory propagations to determine a bank command, is providing the most reliable means of meeting the SE range requirement. Preliminary work on this algorithm was initiated in 1992 to assess long-range low L/D flight for the First Lunar Outpost (FLO).[3] With some major revisions this algorithm (named NSEG) combines the best features of the original high Technology Readiness Level (TRL) Apollo Guidance algorithm[12,13] with a numerical scheme for computing a real-time long-range skip trajectory. NSEG guides the vehicle to a point where the Apollo final-phase logic can take over; i.e., at approximately Mach 23 and an altitude of approximately 200 kft (Figure 11). The Apollo final phase guides the vehicle to a point approximately 7 nmi from the landing site, at about Mach 1.6 and approximately 80-kft altitude.

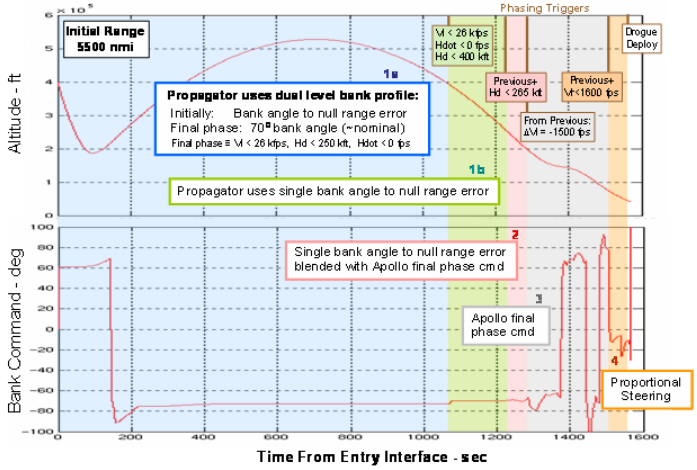

Figure 11. Nominal NSEG Modes of Operation *Shown are altitude and bank angle with superimposed NSEG mode boundaries*

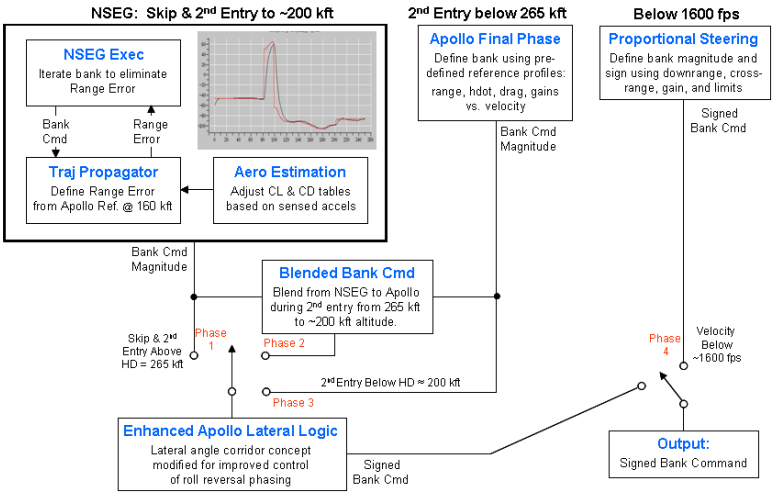

Figure 12. Nominal NSEG Modes of Operation *Shown are typical NSEG guidance phases for a long range skip trajectory.*

The NSEG algorithm is comprised of four main phases as shown in Figure 12.

In phase 1, a numerical solution is generated during the SE until an altitude of approximately 200-kft inbound to the second entry occurs. During phase 1, a skip numeric phase bank-angle command is computed to remove the range errors at 160-kft inbound on the second entry. Early numerical solutions have a built-in performance reserve, implemented by using a bank-angle profile below altitudes of approximately 250-kft inbound to the second entry consistent with the Apollo reference gains. This is currently a 70-degree bank angle. During phase 2, a blended bank-angle command is used to transition the vehicle between the numerical solutions to the Apollo final phase solutions. Finally, below an altitude of approximately 200-kft inbound on the second entry, the guidance enters phase 3 where the Apollo final phase logic is used exclusively. This guidance phase remains active until the vehicle relative speed drops below 1600 feet per second (fps), at which time the proportional steering phase 4 is entered, where a gain proportional to the heading error creates a bank command that guides the vehicle to the desired drogue deployment box. This drogue deployment box is comprised of altitude and range-to-target triggers. Active in all phases except phase 4 is an enhanced Apollo lateral logic module that determines when the vehicle executes a roll reversal.

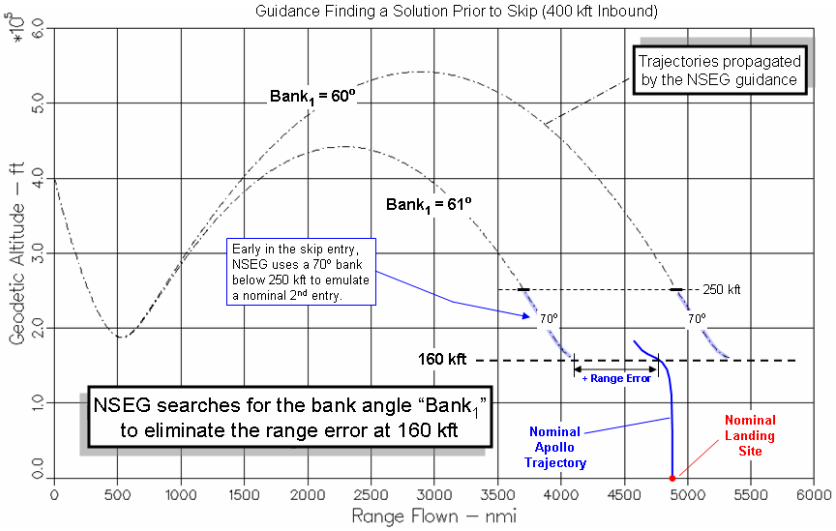

Figure 13. NSEG Bank Solution Illustration *Shown is the one-dimensional NSEG bank iteration search logic.*

NSEG determines bank command magnitude by iteratively propagating constant-bank trajectories to eliminate range error at 160-kft altitude in the Apollo final phase. Figure 12 illustrates the process for a couple of iterations early in SE.

Figure 13 portrays iterations for two bank angles: 61 degrees comes in short of the desired reference Apollo trajectory, while 60 degrees overshoots. Note that both iterations use a 70-degree bank angle for the second entry below 250-kft altitude. This approach is used by NSEG in the initial portion of the SE to force correction of errors early and preserve maneuver capability later in the trajectory. One effect of this approach is to steer out errors that may exist at the first entry interface during the skip, so that the second entry may proceed nominally. Once the inertial velocity drops below 26 kfps, the altitude drops below 400 kft, and the altitude rate becomes negative, the propagator discontinues uses of the dual-level bank profile (Figure 14), and NSEG propagates trajectories with a single, constant bank angle.

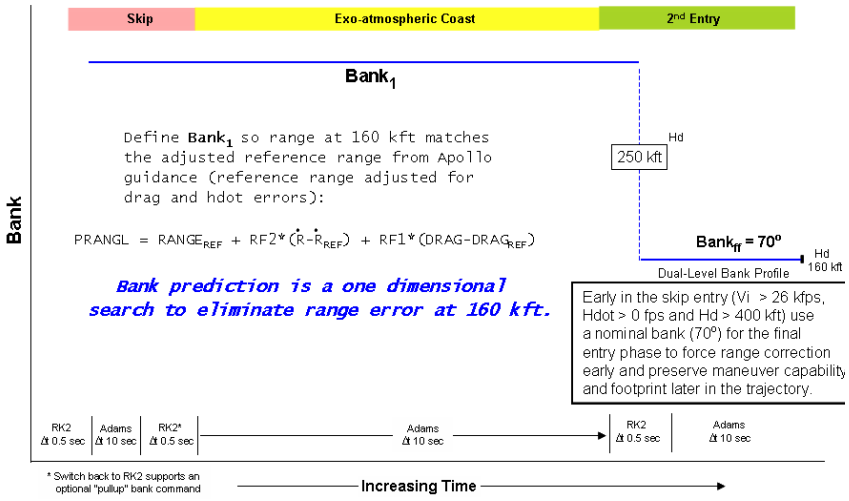

Figure 14. NSEG Dual Lever Bank Angle *Shown are the "early" skip bank angle solution.*

Bank angle is iterated to achieve the compensated reference range at 160 kft on the second entry, as defined by the following equation from the Apollo final phase:

$$RANGE_{COMP} = RANGE_{REF} + GAIN_2*(\dot{R}-\dot{R}_{REF}) + GAIN_1*(DRAG-DRAG_{REF})$$

Definition of the desired bank angle at any point in time then becomes a one-dimensional search so that the range on the propagated trajectory matches the compensated reference range for the Apollo final phase at 160-kft altitude. Currently NSEG uses a bounded Regula-Falsi method to nominally find the solution, as depicted in Figure 15. If difficulties are encountered such that a prediction is made outside of the bounded space, then the search switches to a half-step method to converge on a solution. Each guidance cycle, NSEG must compute its predicted range-to-go at 160-kft altitude (using some assumed environment and bank control). If the predicted range-to-go is different from the desired range (as calculated by the Apollo final phase logic), the commanded bank angle is modified by some appropriate logic, and this process repeats until the predicted range-to-go converges to the desired range.

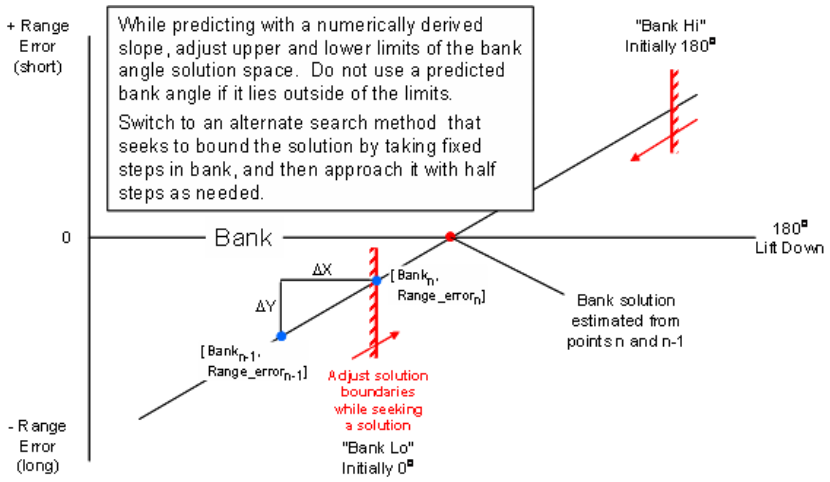

Figure 15. Bank Angle Limiting *Shown is the bank angle limiting approach used during cyclic NSEG convergence.*

In reality, this is a two-dimensional problem, because the goal is to hit a desired range from the landing site with a given latitude and longitude (with heading error to the landing site within specified constraints). However, there is only a single control – commanded bank angle. Although another control could be introduced (e.g., the timing of roll reversals to control out the crossrange), doing so would complicate the convergence of the solution, and would not guarantee that a solution (if one were even to exist) would be found.

Thus, the scalar quantity to be solved for is the range error between the predicted range-to-go and the desired range. NSEG computes its trajectory in-plane (multiplying the lift coefficient by the cosine of the bank angle to get the in-plane contribution to lift, and ignoring the out-of-plane component). Since the landing site exists in the original two-dimensional problem, calculation of the predicted range-to-go at 160 kft is not straightforward, especially when the initial crossrange has not been steered out early in the skip. Range-to-go is therefore calculated as the great circle range from the initial condition (for the propagation) to the landing site minus the great circle range from the initial condition to the terminal condition of the propagation at 160 kft. A positive value indicates the terminal condition is short of the target, while a negative value indicates the terminal condition is past the target.

The implemented range error is then computed as a difference of ranges:

RANGE ERROR = PREDICTED RANGE-TO-GO – DESIRED RANGE

Here, the desired range is computed as the compensated reference range from the Apollo Final Phase logic, as discussed in the previous section. A positive range error means that NSEG is predicting the spacecraft will fall short of the target, while a negative range error means that NSEG is predicting the spacecraft will fly too far. However, a range error of zero does not necessarily mean the spacecraft will fly to the target – it only means the total range it will fly is the range it is supposed to fly. The crossrange corridor logic provides the remaining constraint to insure the vehicle flies to the desired target.

As stated previously, the NSEG guidance law assumes the trajectory lies in a plane. In reality, there could be an initial crossrange component (CRANGA) that must be removed. However, NSEG computes a bank angle assuming the trajectory lays entirely in-plane. In the case of bad dispersions (typically, a lower-than-predicted L/D), the initial crossrange bias cannot be removed during the skip phase, and the bank control during the Apollo phase would be

allocated entirely to meet the downrange constraint. Although some of this control could be reserved for meeting the desired crossrange, it could only come at the cost of increased downrange error.

However, prior to exiting the skip phase, the spacecraft has the control authority to select any range to be flown (Figure 16). But once the skip phase ends, and the Kepler phase begins, the location of the second entry is fixed. So, during the skip phase, we can bias our desired landing site to lie further downrange than it actually does. This biasing, in turn, will shift our second entry point further downrange. If the extra lift is needed, then it will be available, and NSEG will be able to fly out both the downrange as well as the crossrange error. The bias function is chosen as follows:

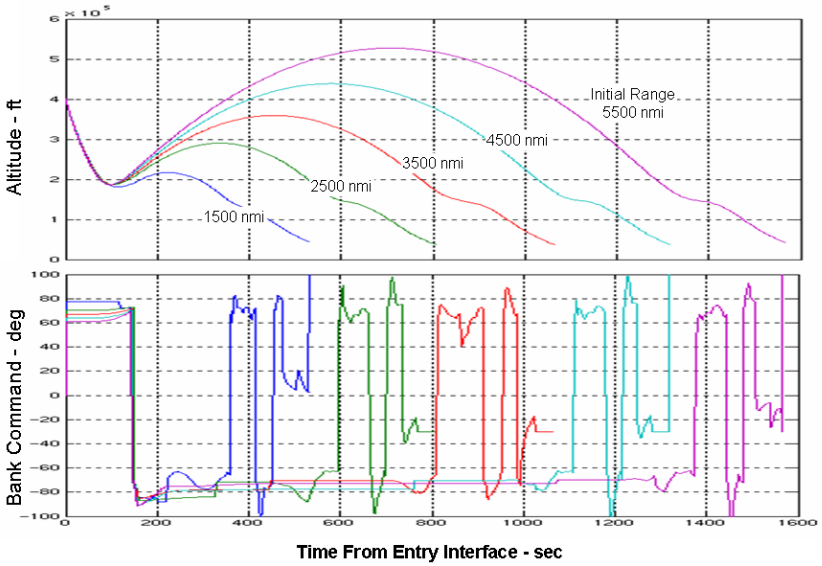

Figure 16. NSEG Ranging Capability *Shown are the bank commands and the associated range flown for various SE trajectories.*

BIASED DESIRED RANGE = DESIRED RANGE +

RBIAS*(ABS (CRANGA)-RBXRL)

(In this function, RBIAS and RBXRL are user-selected I-loads.)

Note that the biasing term disappears as the crossrange approaches the I-load parameter RBXRL. For most cases, this will happen during the skip phase. If this happens, then the crossrange corridor control is no longer a critical issue, and no additional lift needs to be reserved during the skip phase. However, if the SE phase ends and sufficient crossrange has not been removed, then the second entry location will be further downrange than originally planned with the nominal. Thus, less lift is needed to fly out the downrange, and the excess lift can be allocated to flying out the crossrange.

$$\dot{V} = -\frac{D}{M} + g_r - \omega_E^2 r\left[\cos\phi\left(\cos\gamma\sin\phi\cos\psi - \sin\gamma\cos\phi\right)\right] \quad (1)$$

$$V\dot{\gamma} = \left(\frac{V^2}{r}\right)\cos\gamma + g_n + \frac{L}{M}\cos\mu + 2\omega_E V\cos\phi\sin\psi + \omega_E^2 r\left[\cos\phi\left(\cos\gamma\cos\phi + \sin\gamma\sin\phi\cos\psi\right)\right] \quad (2)$$

set = 0 for inplane prediction

$$V\dot{\psi}\cos\gamma = \frac{V^2}{r}\cos^2\gamma\sin\psi\tan\phi - g_w + \frac{L}{M}\sin\mu + 2\omega_E V\left(\cos\gamma\sin\phi - \sin\gamma\cos\phi\cos\psi\right) + \omega_E^2 r\sin\phi\cos\phi\sin\psi \quad (3)$$

Where:

- V Relative velocity
- γ Relative flight path angle
- ψ Relative azimuth from North
- ϕ Declination
- μ Bank angle
- r Radius
- D Drag force
- L Lift force
- M Mass
- ω_E Rotation rate of planet

For a spherical planet:

$g_s = -g_{local} \sin\gamma$

$g_n = -g_{local} \cos\gamma$

$g_w = 0$

For an oblate planet, g_s, g_n, g_w are obtained by transforming gravitational acceleration elements from an earth fixed frame.

References:

MSC Internal Note No. 72-FM-183, MSC-07187, 18 July 1972.
"3-DOF Model: Canonical EOMs", notes from Jeremy Rea/EG5.

Figure 17. NSEG Propagator *Shown are the NSEG propagator equations of motion.*

Furthermore, since the range bias disappears when it is not needed, the crew G-load is not increased unless needed. Shifting the second entry location further downrange causes the second entry bank angle to increase, which results in higher G-loads. But this only happens in the extreme cases that actually need it.

Note that the purpose of this range bias is to reserve enough lift to steer out the crossrange in low L/D (or other extreme) cases. If the initial state has little or no crossrange bias, then this term can easily be turned off by setting RBIAS to 0.

The NSEG propagator models motion relative to a rotating planet using the classical equations identified in Figure 17. Note that the NSEG propagator is only used to evaluate in-plane ranging; the effect of lift and bank on the rate of change of azimuth [see equation (3) in Figure 17] is therefore ignored.

A six-element state is propagated: relative velocity, relative flight path angle, relative azimuth, radius, longitude, and declination. The derivatives of the first three terms are calculated from the equations in Figure 17. The derivatives of radius, longitude, and declination are calculated as follows:

$$\dot{r} = V \sin\gamma$$

$$\dot{\lambda} = \frac{V \cos\gamma \sin\psi}{r \cos\phi}$$

$$\dot{\phi} = \frac{V \cos\gamma \cos\psi}{r}$$

The derivatives are then integrated numerically using a fourth-order Adams Bashforth – Adams Moulton predictor-corrector, with a second-order Runge Kutta (RK) starter algorithm. Satisfactory performance has been obtained using a one-half-second time step for the RK algorithm, and a 10-second time step for the predictor-corrector. When a trajectory is propagated for a "dual-segment" bank profile, a switch is made from the predictor-corrector back to the RK (and its smaller time step) to provide more consistent range errors from one iteration to the next; i.e., by changing bank angle as close to 250-kft altitude as practical for each iteration. Following the bank-angle change, the propagator reverts to the predictor-corrector.

The propagator equations were validated with trajectories generated by another tool, Simulation and Optimization of Rocket Trajectories (SORT)[1]. SORT provided a solid means of independent validation, since it propagates using an Earth-centered inertial coordinate system, and a fourth-order RK algorithm. An excellent comparison was obtained between SORT and NSEG, when comparable atmosphere and gravity models were used.

The propagator uses simplified models for atmospheric density and speed of sound, the aerodynamic coefficients, gravity, and planet flattening. Atmospheric density is modeled using two polynomials that define the natural log of density versus altitude. A third-order polynomial is used for the initial skip phase, while a fifth-order polynomial is used for the second entry. Coefficients for these polynomials are defined by curve-fitting data from nominal trajectories generated use the Global Reference Atmosphere Model-99 (GRAM-99)[9] atmosphere model for the expected entry conditions. Note that NSEG performance is sensitive to the skip atmosphere, especially for initial ranges of approximately 5000 nmi and greater; i.e., a skip atmosphere that delivers good performance for one initial latitude and season will not necessarily provide the same level of performance for another. Speed of sound (for definition of Mach number) is modeled using a simple linear table lookup from six data points versus altitude. The propagator uses tables of CL and CD versus Mach, for possible trim conditions. The propagator is currently configured with tables for trim L/Ds from 0.25 to 0.50 with the expected nominal condition specified by user defined I-loads. Adjustments from the anticipated nominal are

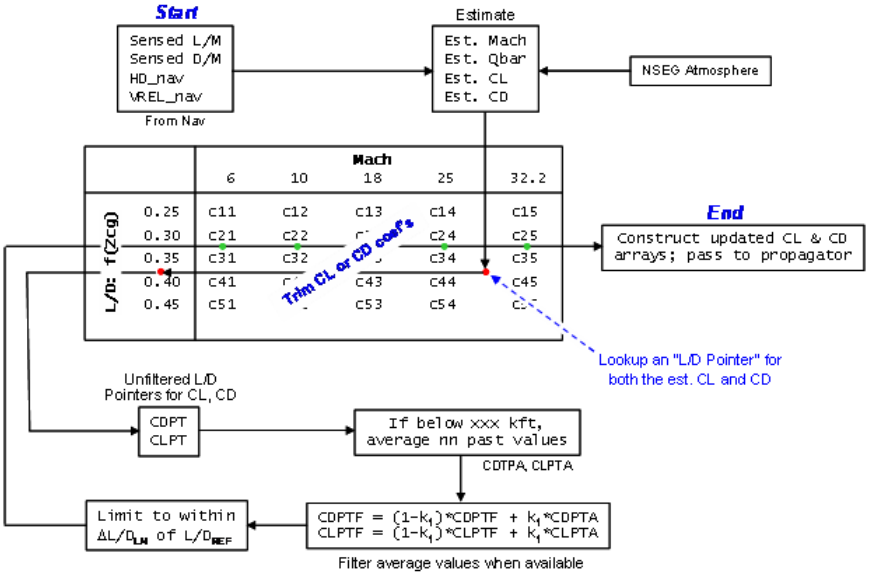

Figure 18. Aero Estimation Logic *A schematic is shown illustrating the process used to obtain real-time aero coefficient estimations.*

currently done using navigation derived data, as described in the next section. The gravity model currently includes J2 effects only.

Uncertainty in the longitudinal aerodynamic coefficients (the lift, drag, and pitching moment coefficients) and the CG location plays a big role in defining the performance limitations of the NSEG algorithm. It was estimated that the effect of aero and CG uncertainty on NSEG performance was 1.5 to 2 times that of all the other uncertainties combined. Given that, it was decided to reduce the effect of the aero uncertainty by including a real-time adjustment of the aero coefficients in the NSEG propagator. The approach (Figure 18) averages and filters data derived from sensed lift and drag accelerations.

The approach does not try to explicitly distinguish the individual effects of the aero uncertainties and atmospheric dispersions on the sensed accelerations; i.e., the accelerations are translated into aero coefficients using the NSEG models of the nominal atmosphere. However, since the effect of aero uncertainty is dominant, the approach offers a significant improvement in NSEG performance, especially for initial ranges of 4900–5400 nmi, required for the worst-case Earth-Moon geometries. For example, with the aero estimation logic, range at drogue deploy is less than 1 nmi for all 3000 MC samples to the prime and weather-alternate landing sites. Without the aero estimation logic, and an initial range of 4910 nmi, there are 34 range misses greater than 2 nmi, 8 misses over 100 nmi, with the worst being 420 nmi.

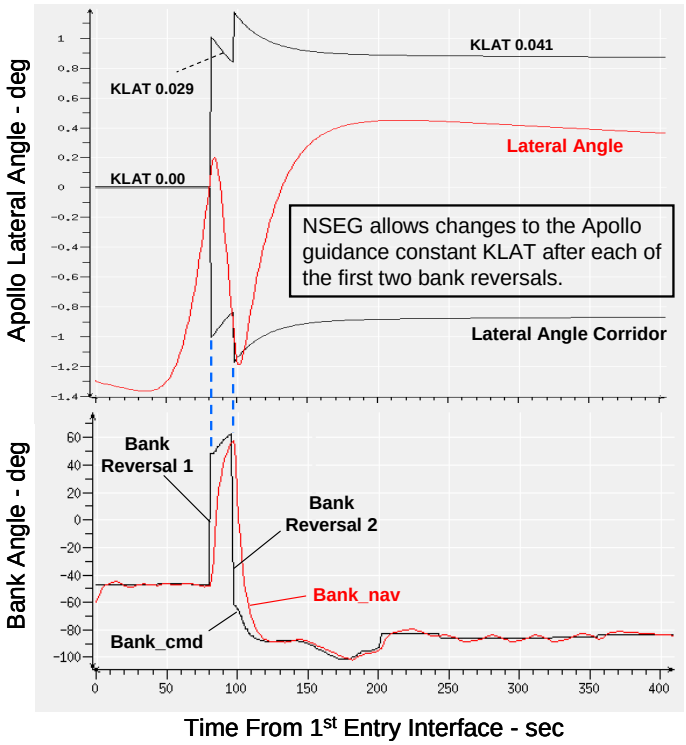

Figure 19. Lateral Angle Corridor *Shown are adjustments made to increase flexibility of the baseline lateral corridor logic.*

For the most part, the fundamental approach to controlling heading error to the target, and determining timing of the bank reversals, is the same as in Reference 12. However, some small changes were made in order to allow more flexibility in phasing the initial bank reversals for the preplanned, nominal trajectory. The changes follow the approach used in Shuttle Entry Guidance, where the width of the heading error corridor expands after the first reversal. In the case of NSEG, flexibility was added to adjust the corridor after both the first and second bank reversal (Figure 19). In general, the constants that define the lateral corridor (labeled "KLAT" in Figure 19) are chosen so that the lateral angle (and hence crossrange) are small or slightly positive for the second entry (see Figure 20). Currently, a set of unique KLATs are defined for the planned initial downrange and crossrange.

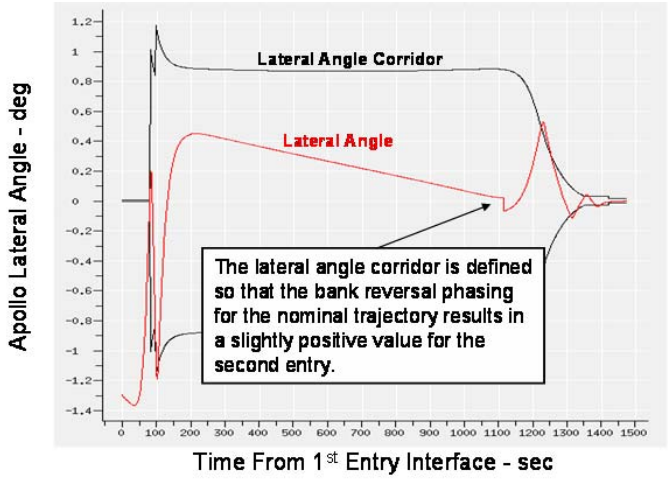

Figure 20. Nominal lateral logic targeting *Small second entry crossrange capability is targeted.*

Another change to the lateral logic involves specifying the rotational direction of the early bank reversals; i.e., specifying that the reversal results in the lift vector passing through vertical in either an up or down orientation. Early reversals at super-circular velocities can safely be done "lift-vector-up", as long as a high L/D ratio or some other high-energy dispersion is not present. However, if a high-energy condition is detected, it is best to perform a bank reversal "lift-vector-down" to avoid having the reversal add energy to the trajectory and induce

excessively high loads during the second entry. Currently, high-energy conditions are assessed by examining the magnitude of the bank command at the time of the reversal. If the bank command magnitude exceeds a specified value (e.g., 82 degrees), and the current inertial velocity is greater than some value (e.g., 26 kfps), the reversal is commanded lift-vector-down.

With the exception of the lateral enhancements noted in the prior section, the approach to the Apollo Final Phase follows that defined in Reference 12. The logic, gains, and reference trajectory constants are virtually unchanged from those used in the Apollo era. Enhancements to the gains, reference trajectory constants, and the associated logic are being considered.

A proportional steering controller is used to guide the vehicle directly toward the landing site during the terminal phase. Proportional steering currently has two phases. The first phase is initiated at a specified relative velocity (e.g., 1600 fps), where a gain is applied to the Apollo lateral angle (or heading error) to define the bank command. The second phase is initiated at a lower velocity (e.g., 800 fps), where a gain is applied to the inverse tangent of the ratio of crossrange to downrange to define the bank command. Both phases limit the magnitude of the bank command to independent specified values. It may be possible to use only the second phase, but that option has not yet been assessed.

V. Nominal Flight Results

The 3-DOF SORT simulation was used to establish the nominal performance of the NSEG algorithm. This was accomplished by flying trajectories that all started at a fixed EI condition, using a 76 standard atmosphere, holding the vehicle aerodynamics at their nominal values, and freezing the guidance initialization load. A "raster-scan" was then performed where the target drogue deployment point was moved over the surface of the Earth and a flight was generated to that target site. Figure 21 provides the color-coded results of this analysis. Each color pixel on the chart indicates the miss distance from the targeted drogue deployment point. All red colored pixels indicate a target miss of less than 0.25 nmi; yellow colored pixels indicate a miss between 0.25 and 1 nmi; green pixels indicate a miss from 1 to 2.5 nmi; shades of blue indicate misses from 2.5 to 10 nmi; cyan colored indicate miss distances less than 60 nmi; and white pixels indicate misses greater than 60 nmi. Figure 21 shows the results of 95,000 flights spanning ranges up to 7,000 nmi from EI. All flights were done with zero azimuth (i.e., polar flights parallel to meridians of longitude) which resulted in the asymmetry of the plot about zero crossrange.

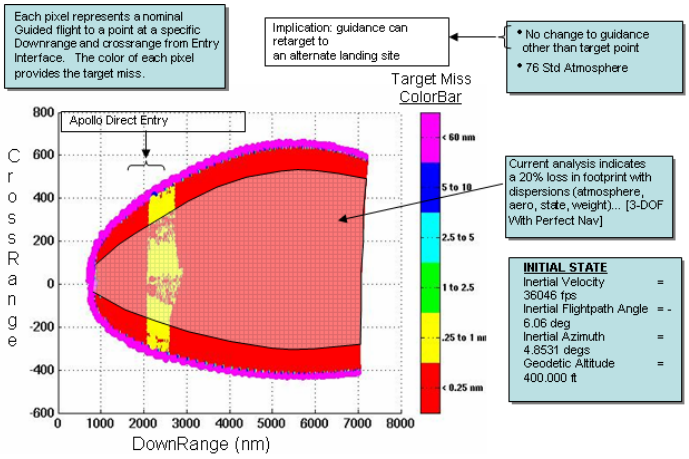

Figure 21. Nominal NSEG Capability Footprint *Shown is nominal NSEG drogue chute target acquisition performance .*

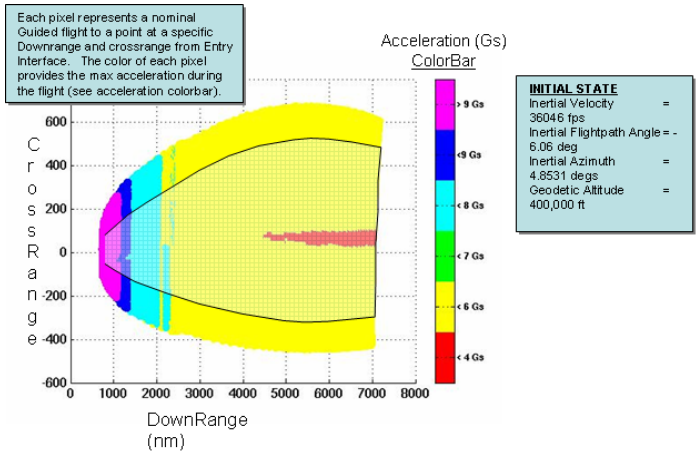

Figure 22. Nominal NSEG Acceleration Footprint *Shown is nominal NSEG drogue chute target G-load performance.*

Noteworthy within Figure 21 is the stability of the algorithm across the scanned range and crossrange. No performance gaps are found. The yellow region in this plot highlights a performance shift of approximately one-half nautical mile, and indicates the internal guidance mechanization required for flights that transition between short-range final phase Apollo guidance only to longer skip ranges requiring the combined

numerical NSEG solution and final phase Apollo guidance solution. This plot was generated for a vehicle with 0.4 L/D, or approximately 12 percent higher than the 0.35 L/D vehicle flown as discussed in Section VI of this report.

Figure 22 provides the maximum acceleration (G-loads) during flight for each of the 95,000 flights. Short-range flights provide maximum G-loads consistent with the use of the original Apollo guidance logic. Longer-range flights reduce the G-loads, as integral effect of the velocity reduction occurs over a longer period of time and is split between the SE and second entry.

VI. Dispersed Flight Results

The Architecture for Exploration Studies (ARES) simultor was used to evaluate the dispersed NSEG flight performance. ARES is a 6-DOF simulation tool that provides a realistic simulation environment. It is comprised of a library of vehicle generic models and vehicle specific models defined for the CEV. It is currently configured for phase-specific simulations – ascent, on-orbit, and entry. While the ARES simulation is constantly improving, ARES V6.3 will be used for the analysis of the NSEG algorithm. However, ARES V6.5 will be used to investigate Reaction Control System (RCS) mass consumption.

EI Condition	Ops Site 1	Ops Site 2	Ops Site 3	Ops Site 4
Geodetic Latitude	-47.0789º	-26.2869 º	-6.98043 º	15.6016 º
Longitude	-112.552 º	-113.805 º	-150.113 º	-171.51 º
Geodetic Altitude (ft)	400,000	400,000	400,000	400,000
Inertial Velocity (fps)	36046	36046	36046	36046
Inertial Flightpath	-6.06 º	-6.06 º	-6.06 º	-6.06 º
Inertial Azimuth	0 º	0 º	32.2642 º	55.9743 º
Inclination	90 º	90 º	58 º	37 º
Range to Targeted Landing Site (n.mi)	5250 - UTTR **4910 - EAFB** 5310 - GRV	4010 - UTTR **3660 - EAFB** 4060 – GRV 3960 - CAR	3640 - UTTR **3230 - EAFB** 3440- GRV 3440 - CAR	3540 - UTTR **3290 - EAFB** 3300 - CAR
Crossrange to Targeted Landing Site (n.mi)	250 - UTTR **30 - EAFB** -80 - GRV	240 - UTTR **20 - EAFB** -90 – GRV 16 - CAR	140 - UTTR **220 - EAFB** -145 – GRV 8 - CAR	-220 - UTTR **100 - EAFB** -194 - CAR

Table 1. MC Operational Site Data Sets *Shown are the 4 operational sites chosen as initial EI states for the detailed 6-DOF analyses. Also included are the range and crossrange to the primary and alternate landing sites.*

Critical Parameter	*Dispersion*	*Mean*	*3 σ / Max*	*Basis for 3 σ Values*
EI Altitude	Uniform	400,000 ft	+/- 500 ft	X-38 Program
EI Latitude / Longitude	Uniform	Varies	+/- 0.2 deg	X-38 Program
Entry Velocity	Gaussian	36,046 fps (10,986 mps)	90 fps (27.4 mps)	
Entry Flight Path Angle	Gaussian	-6.06 deg	0.1 deg	Dispersion based on 0.5 n.mi vacuum periapse altitude error (Source: Apollo NASA SP-8015)
EI Azimuth	Uniform	Varies	+/- 0.05 deg	X-38 Program
Atmospheric Density and Winds	-	-	Gram seed	GRAM-99 Atmosphere Model
Aero Coefficient Factor: CL, CD, Cm	Gaussian	-	Varies with Mach number Un-correlated	"Aerodynamic Design Data Book for the Crew Exploration Vehicle, Ver. 0.1," CAP Aerodynamic Team, May 2006 Section 4.4.1: "They are based on a bounding of historical uncertainties from lifting bodies such as 24 and X-38, Orbiter, X-33, and other programs."
Navigation	-	Varies		GPS/INS/FADS HiFi w/ blackout (Source: Boeing STS 83-0004-30-A, Also TM-02-0006-05
Vehicle Mass	Uniform	16,354 lbm	+/- 3.1%	
Vehicle Inertia	Gaussian	DAC2	+/- 3.1%	Inertia dispersions are correlated
Center-of-Gravity	Gaussian	DAC2 (mod for L/D = 0.35)	Xcg: 0.5" Ycg: 0.3" Zcg: 0.3"	Nominal: Xcg = 1053.2" (ARES Frame) Ycg = 0.2" Zcg = 8.3" (L/D = 0.35)
RCS Jet Thrust	Uniform	160 lbf	+/- 5.0%	

Table 2. ARES Monte-Carlo Dispersion Magnitudes. *Shown is the ARES model dispersions applied for each 6-DOF MC sets of analyses.*

To assess the SE capability, four operational entry interface data sets (MC_OPS1-4) have been selected as target locations for the Trans-Earth Injection (TEI) and Trajectory Control Maneuver (TCM). These locations will be used to initialize MC simulations to test the objective of returning the crew from the full range of possible lunar return antipodes and access primary and weather-alternate landing sites. The reason for choosing these four operational MC-site locations was explained previously and shown graphically in Figures 5-7 with detailed Initial Conditions (ICs) provided in Table 1. The detailed data provided in this table for each MC_OPS set includes the targeted EI state vector, the landing site target options, and the range and crossrange at EI to these sites. For this analysis, the MC-OPS site will be held constant for each target location specified in Table 1. This will assess the feasibility of allowing the lunar return crew to re-designate to an alternate landing site while within close proximity EI.

SE performance using NSEG was assessed over the possible dispersed conditions summarized in Table 2. Three-thousand randomly dispersed cases were generated for the prime and two weather-alternate sites for each of the four possible initial conditions (Ops Site 1-4).

	Ops Site 1			Ops Site 2		
	UTTR	EAFB	GRV	UTTR	EAFB	GRV
	5250,250	4910,30	5310,-80	4010,240	3660,20	4060,-90
0 - 1 n.mi. =	3000	3000	3000	3000	3000	3000
1 - 1.5 n.mi. =	0	0	0	0	0	0
1.5 - 2 n.mi. =	0	0	0	0	0	0
2 - 5 n.mi. =	0	0	0	0	0	0
5 - 10 n.mi. =	0	0	0	0	0	0
10 - 50 n.mi. =	0	0	0	0	0	0
50 - 1000 n.mi. =	0	0	0	0	0	0
Klat1	0.002	0.041	0.0001	0.017	0.041	0.001
Klat2	0.041	0.041	0.041	0.041	0.041	0.041
Klat3**	na	na	0.029	na	0.027	0.025
Rrdwn	82	82	82	90	82	82
Rbias	15/100	10/55	3/55	5/100	3/55	0/55
Tnom	1500	1500	1500	1050	1050	1050

** when specified, used after 1st RR. Klat2 is then used after 2nd RR.

Table 3. Monte-Carlo Results. *Three thousand case MC results and I-Load changes for OPS sites 1 and 2*

	Ops Site 3			Ops Site 4		
	UTTR	EAFB	GRV	UTTR	EAFB	CAR
	3640,140	3230,220	3440,-145	3540,-220	3290,100	3300,-194
0 - 1 n.mi. =	3000	3000	3000	3000	3000	3000
1 - 1.5 n.mi. =	0	0	0	0	0	0
1.5 - 2 n.mi. =	0	0	0	0	0	0
2 - 5 n.mi. =	0	0	0	0	0	0
5 - 10 n.mi. =	0	0	0	0	0	0
10 - 50 n.mi. =	0	0	0	0	0	0
50 - 1000 n.mi. =	0	0	0	0	0	0
Klat1	0.037	0.019	0.040	0.023	0.005	0.027
Klat2	0.041	0.041	0.041	0.041	0.041	0.041
Klat3**	na	na	na	na	na	na
Rrdwn	90	82	82	90	82	90
Rbias	2/100	2/100	2/100	2/100	0/100	2/100
Tnom	1050	1050	1050	1050	1050	1050

** when specified, used after 1st RR. Klat2 is then used after 2nd RR.

Table 4. Monte-Carlo Results. *Three thousand case MC results and I-Load changes for OPS sites 3 and 4*

	Ops Site 1			Ops Site 2		
	UTTR	EAFB	GRV	UTTR	EAFB	GRV
Maximum Dynamic Pressure - Skip (psf)						
Maximum	459	465	454	477	484	472
Minimum	343	348	343	337	340	332
Mean	394	401	392	391	394	386
Median	393	400	391	391	394	386
Std Deviation	17	18	17	19	19	19
Maximum Dynamic Pressure - 2nd Entry (psf)						
Maximum	698	486	556	433	396	404
Minimum	239	230	235	260	267	253
Mean	355	334	322	347	331	323
Median	353	333	318	345	330	322
Std Deviation	48	33	41	27	18	26
Maximum Chapman's Heat Rate - Skip (btu/ft2/sec)						
Maximum	677	681	678	692	695	689
Minimum	587	590	588	574	577	571
Mean	626	630	626	621	623	619
Median	626	629	626	621	623	619
Std Deviation	14	14	14	15	15	15
Maximum Chapman's Heat Rate - 2nd Entry (btu/ft2/sec)						
Maximum	234	220	228	227	206	216
Minimum	178	177	168	172	170	167
Mean	204	199	197	195	189	191
Median	204	200	197	196	190	191
Std Deviation	8	8	9	8	6	8
NSEG Bank Command - 2nd Entry (deg)						
Maximum	104.5	89.8	97.0	75.1	76.6	79.6
Minimum	23.2	51.2	56.6	44.1	63.9	67.5
Mean	70.6	70.4	71.5	70.1	71.2	72.0
Median	70.4	70.2	71.1	70.2	71.1	71.9
Std Deviation	4.2	2.6	2.8	1.1	1.7	1.5

Table 5. Statistical Results for Ops Site 1 and 2. *Three thousand case MC statistical results.*

	Ops Site 1			Ops Site 2		
	UTTR	EAFB	GRV	UTTR	EAFB	GRV
Maximum Dynamic Pressure - Skip (psf)						
Maximum	459	465	454	477	484	472
Minimum	343	348	343	337	340	332
Mean	394	401	392	391	394	386
Median	393	400	391	391	394	386
Std Deviation	17	18	17	19	19	19
Maximum Dynamic Pressure - 2nd Entry (psf)						
Maximum	698	486	556	433	396	404
Minimum	239	230	235	260	267	253
Mean	355	334	322	347	331	323
Median	353	333	318	345	330	322
Std Deviation	48	33	41	27	18	26
Maximum Chapman's Heat Rate - Skip (btu/ft2/sec)						
Maximum	677	681	678	692	695	689
Minimum	587	590	588	574	577	571
Mean	626	630	626	621	623	619
Median	626	629	626	621	623	619
Std Deviation	14	14	14	15	15	15
Maximum Chapman's Heat Rate - 2nd Entry (btu/ft2/sec)						
Maximum	234	220	228	227	206	216
Minimum	178	177	168	172	170	167
Mean	204	199	197	195	189	191
Median	204	200	197	196	190	191
Std Deviation	8	8	9	8	6	8
NSEG Bank Command - 2nd Entry (deg)						
Maximum	104.5	89.8	97.0	75.1	76.6	79.6
Minimum	23.2	51.2	56.6	44.1	63.9	67.5
Mean	70.6	70.4	71.5	70.1	71.2	72.0
Median	70.4	70.2	71.1	70.2	71.1	71.9
Std Deviation	4.2	2.6	2.8	1.1	1.7	1.5

Table 6. Statistical Results for Ops Site 3 and 4. *Three thousand case MC statistical results.*

Tables 3 and 4 provide the results of this analysis and indicate that all 3000 cases, for each of the 12 situations, deploy the drogue chute within 1 nmi of the target. Note that these figures identify the changes to the lateral corridor I-loads (the KLATs), the value used to trigger lift-down roll reversals above 26 kfps (Rrdwn), the range bias gain and threshold (Rbias), and the nominal flight time for crossrange initialization (Tnom).

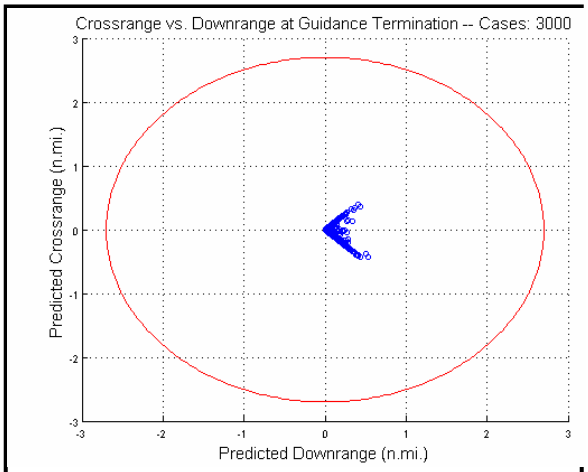

Figure 23. Ops Site 1: UTTR. *Drogue deploy conditions at Utah Test Range (3000 cases).*

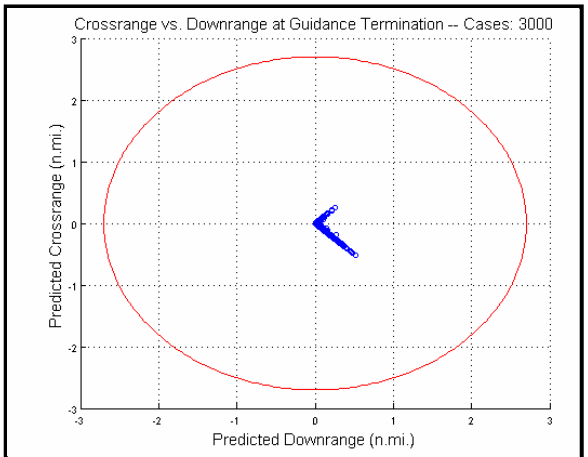

Figure 24. Ops Site 1: EAFB. *Drogue deploy conditions for Edwards Air Force Base (3000 cases).*

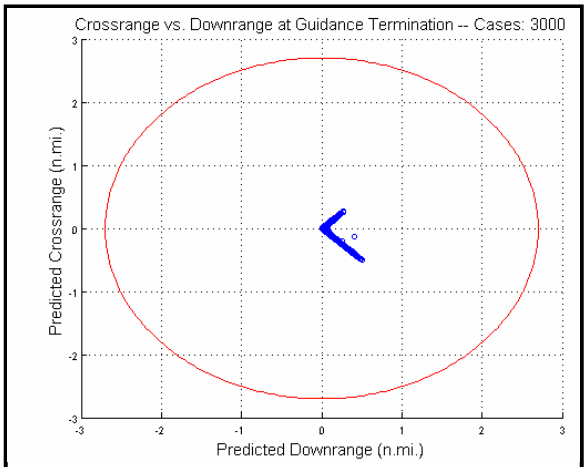

Figure 25. Ops Site 1: GRV. *Drogue deploy conditions at Graves Valley (3000 cases).*

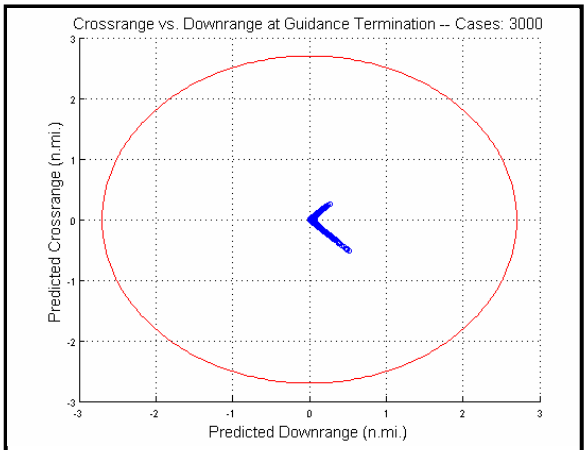

Figure 26. Ops Site 2: UTTR. *Drogue deploy conditions at Utah Test Range (3000 cases).*

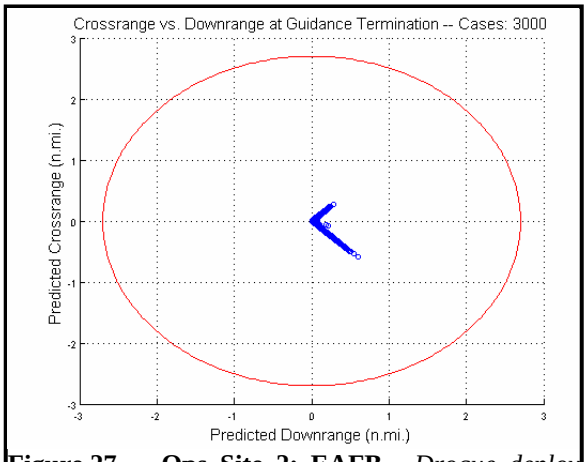

Figure 27. Ops Site 2: EAFB. *Drogue deploy conditions at Edwards Air Force Base (3000 cases).*

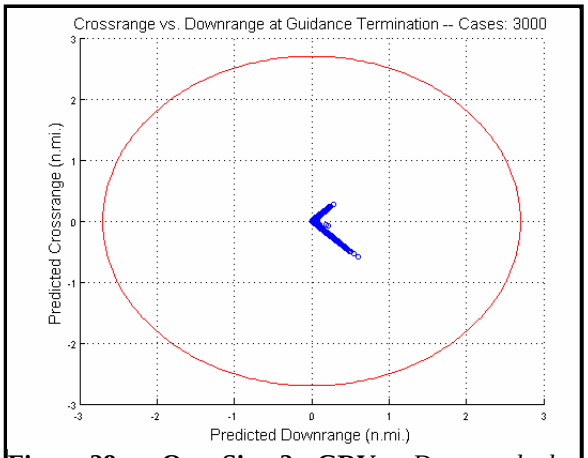

Figure 28. Ops Site 2: GRV. *Drogue deploy conditions at Graves Valley (3000 cases).*

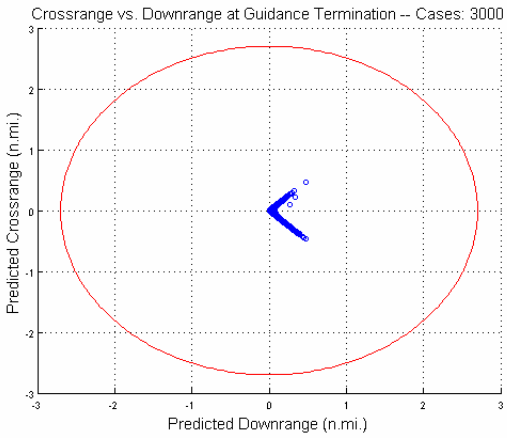

Figure 29. Ops Site 3: UTTR. *Drogue deploy conditions at Utah Test Range (3000 cases).*

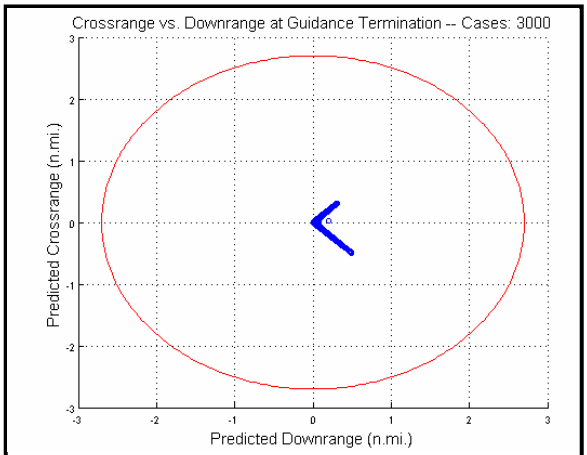

Figure 30. Ops Site 3: EAFB. *Drogue deploy conditions at Edwards Air Force Base (3000 cases).*

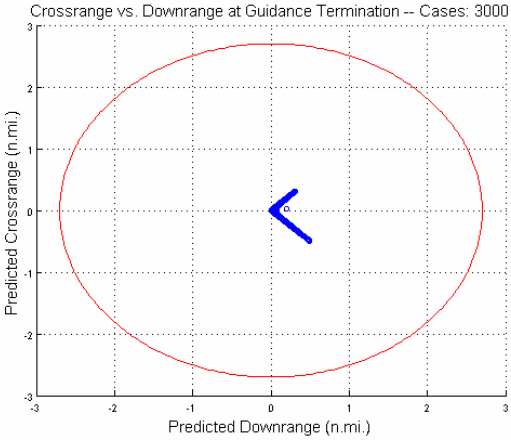

Figure 31. Ops Site 3: GRV. *Drogue deploy conditions at Graves Valley (3000 cases).*

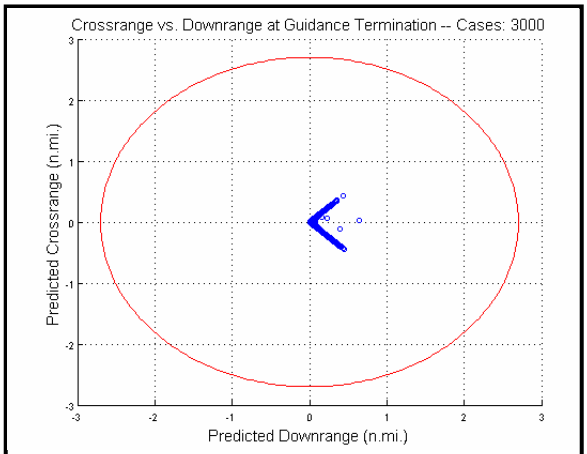

Figure 32. Ops Site 4: UTTR. *Drogue deploy conditions at Utah Test Range (3000 cases).*

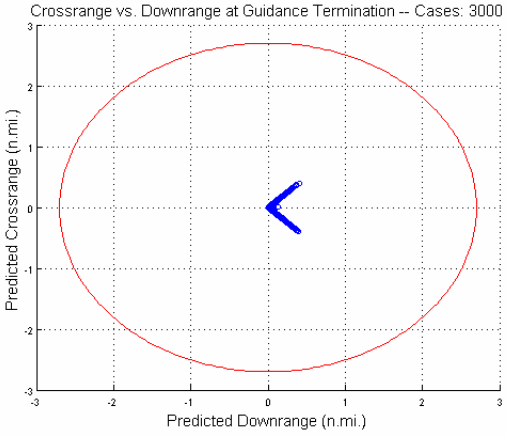

Figure 33. Ops Site 4: EAFB. *Drogue deploy conditions at Edwards Air Force Base (3000 cases).*

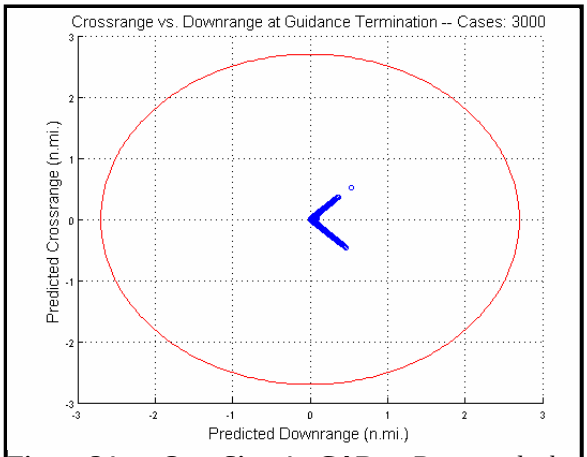

Figure 34. Ops Site 4: CAR. *Drogue deploy conditions at Carson Flat e (3000 cases).*

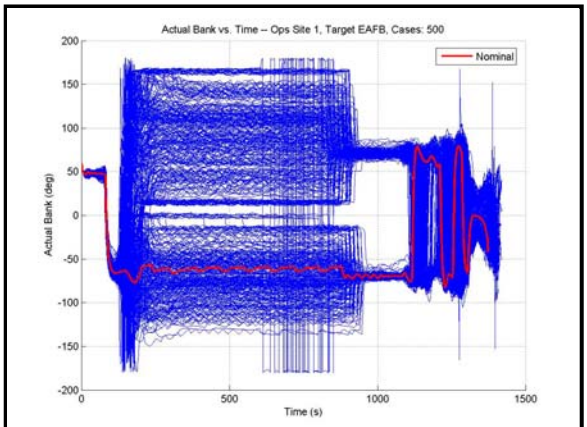

Figure 35. Ops Site 1: EAFB. *Actual NSEG bank angle versus Time from EI (500 cases)*

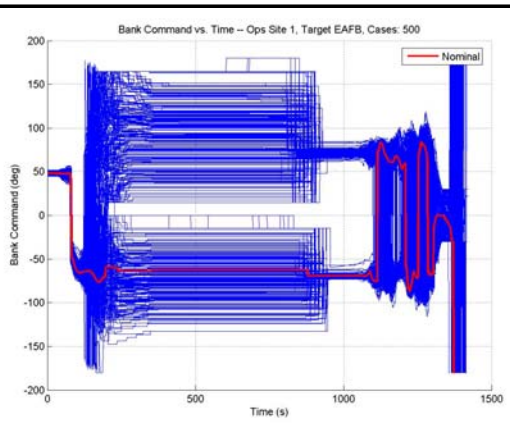

Figure 36. Ops Site 1: EAFB. *Commanded NSEG bank angle versus Time from EI (500 cases)*

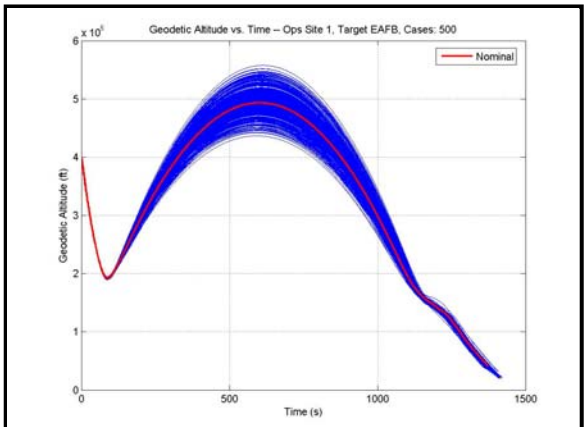

Figure 37. Ops Site 1: EAFB. *Geodetic Altitude versus Time (500 cases)*

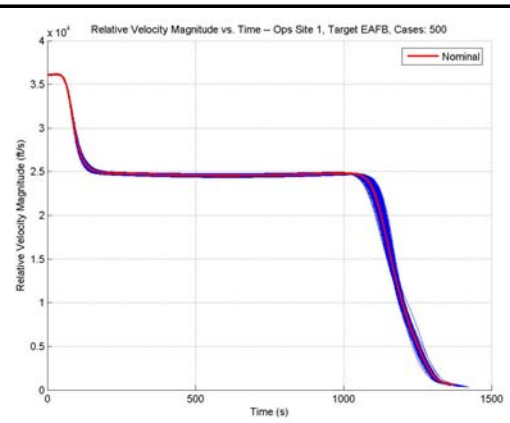

Figure 38. Ops Site 1: EAFB. *Relative Velocity Magnitude versus Time (500 cases)*

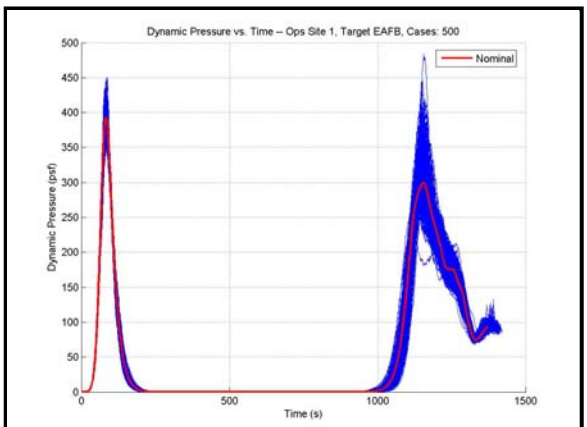

Figure 39. Ops Site 1: EAFB. *Dynamic Pressure versus Time (500 cases)*

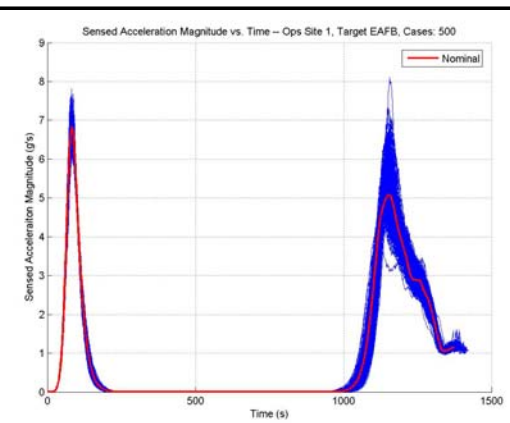

Figure 40. Ops Site 1: EAFB. *Relative Velocity Magnitude versus Time (500 cases)*

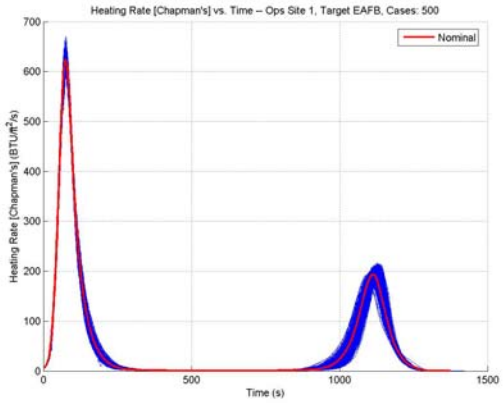

Figure 41. Ops Site 1: EAFB. *Chapman's Heating Rate versus Time (500 cases)*

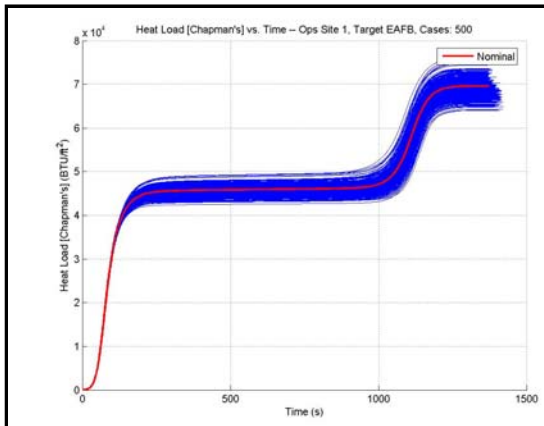

Figure 42. Ops Site 1: EAFB. *Chapman's Heat Load versus Time (500 cases)*

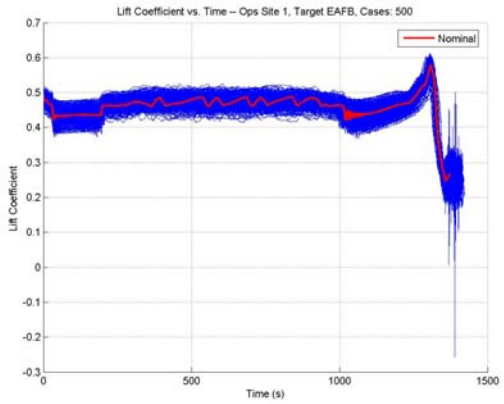

Figure 43. Ops Site 1: EAFB. *Lift Coefficient versus Time (500 cases)*

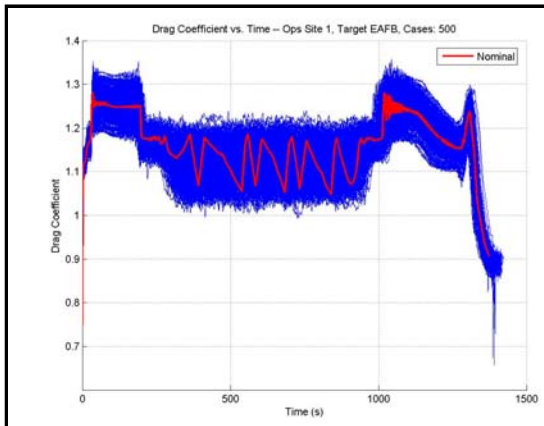

Figure 44. Ops Site 1: EAFB. *Drag Coefficient versus Time (500 cases)*

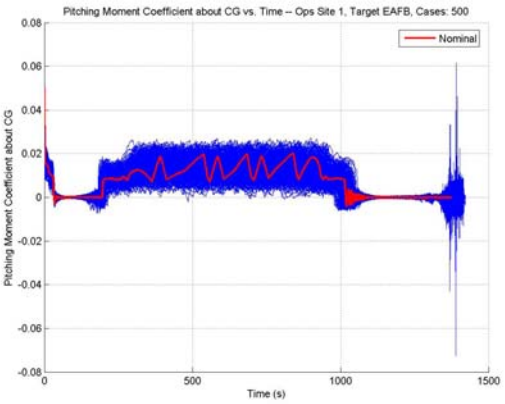

Figure 45. Ops Site 1: EAFB. *Pitching Moment versus Time (500 cases)*

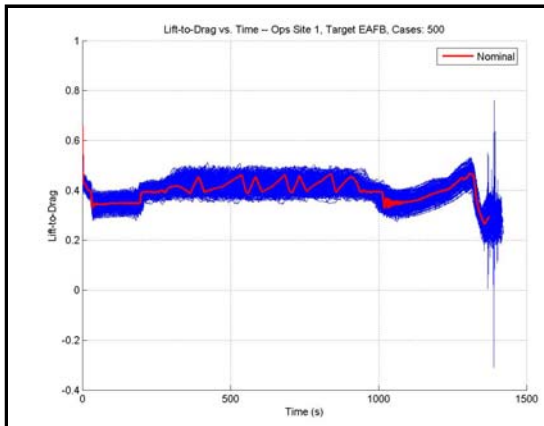

Figure 46. Ops Site 1: EAFB. *Lift-to-Drag Ratio versus Time (500 cases)*

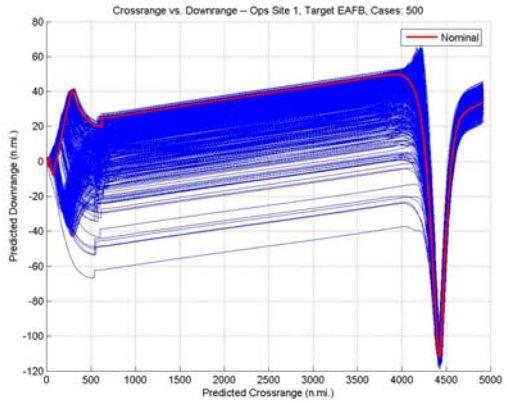

Figure 47. Ops Site 1: EAFB. *DownRange versus Crossrange (500 cases)*

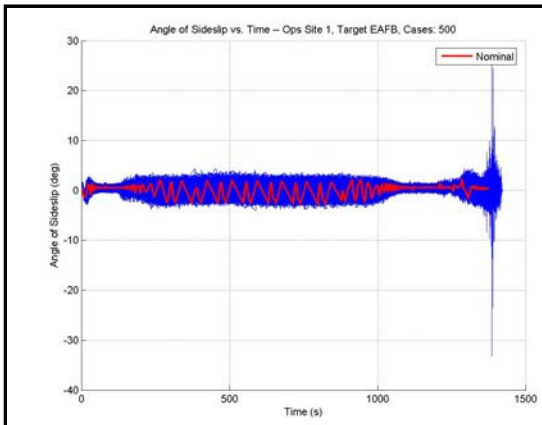

Figure 48. Ops Site 1: EAFB. *Angle-of-Attack versus Time (500 cases)*

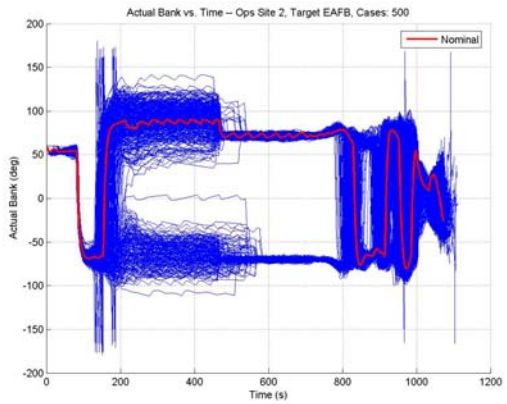

Figure 49. Ops Site 2: EAFB. *Actual Bank vs Time (500 cases)*

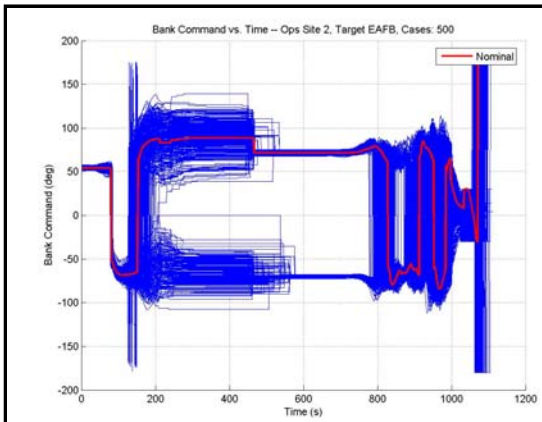

Figure 50. Ops Site 2: EAFB. *Commanded Bank Angle versus Time (500 cases)*

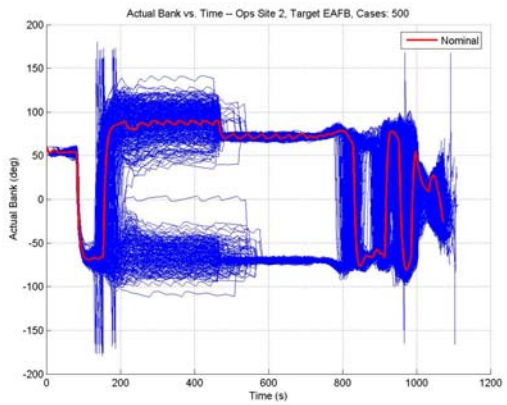

Figure 51. Ops Site 3: EAFB. *Actual Bank vs Time (500 cases)*

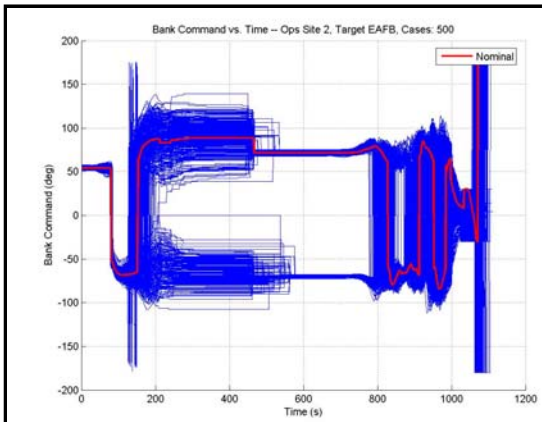

Figure 52. Ops Site 3: EAFB. *Commanded Bank Angle versus Time (500 cases)*

VII. Conclusion

- An approach proposed for providing continuous single Continental United States landing site access for capsule vehicles throughout the lunar month utilizing lunar TEI co-azimuth and trip time control.
- A numerical Skip-Entry guidance algorithm (NSEG) has been assessed that provides single and weather alternate CONUS landing site access throughout the lunar month..
- Acceptable SE flight and landing site performance was provided without using an exo-atmospheric correction maneuver.
- A capsule vehicle with lift-to-drag capability in the 0.35-0.4 range has been shown adequate to enable SE flight trajectories.
- The proposed SE technique permits re-designation to an alternate landing site in close proximity to the earth Entry Interface.

References

[1]Berning, M. J., Sagis, K. D.,"User's Guide for the Simulation and Optimization of Rocket Trajectories (SORT) Program Version 7", Contract NAS 9-17900, October 1992.

[2]Bryant, L. E., "Skip Trajectory Analysis (Providing Global Mars Access)", NASA/JSC Briefing, August 8, 2001.

[3]McCleary, B., Crull, T., Schmitt, L., Wood, R., "Lunar Return Footprint Assessment Using Apollo Guidance". McDonnell Douglas Space Systems Company, Houston Division, Guidance Navigation & Control Internal Report, Feb. 1992.

[4]Chapman, D.,"An Analysis of the Corridor and Guidance Requirements for Super Circular Entry into Planetary Atmospheres", NASA Technical Report R-55, 1960.

[5]Dawn, T. F., Langan, M. P., "Earth Return Trajectory Design Study for the First Lunar Outpost Mission", NASA Report JSC-26141, January 1993.

[6]Detra, R. W., Kemp, N. H., Riddell, F. R., "Heat Transfer to Satellite Vehicles Re-entering the Atmosphere," ARS 11th Annual Meeting, New York, N. Y., 1956.

[7]Graves, C. A., Harpold, J. C., "Apollo Experience Report: Mission Planning for Apollo Reentry", MSC Internal Note No. 70-FM-155, October 5, 1970.

[8]Harpold, J. C., Graves, C. A., "Shuttle Entry Guidance", Journal of the Astronautical Sciences, Vol. XXV11, No.3, pp. 239-268, July-September, 1979.

[9]Justus, C., Johnson, D., "The NASA/MSFC Global Reference Atmospheric Model – 1999 Version (GRAM 99)", NASA Technical Memorandum - 1999-209630, May 1999

[10]Long, A. D., McHenry, R. L., "Shuttle Powered Flight Guidance Equations Development", NASA Report JSC-19995, August 1984.

[11]McCleary, B., Crull, T., Schmitt, L., Wood, R., "Lunar Return Footprint Assessment Using Apollo Guidance", McDonnell Douglas Space Systems Company, Houston Division, Guidance Navigation & Control Internal Report, February, 1992.

[12]Moseley, P. E., Morris, R. L., "The Apollo Entry Guidance: A Review of the Mathematical Development and its Operational Characteristics", Task MSC/TRW A-220, December 1969.

[13]TRW Note No. 69-FMT-791, "The Apollo Entry Guidance: A Review of the Mathematical Development and Its Operational Characteristics", December 1, 1969, Sections 5.3 and 6.4.

[14]"Report on the 90-Day Study on Human Exploration of the Moon and Mars", NASA, November 1989

[15]Peterson, W. L., Dawn, T., Tigges, M. A., et al., "Earth Land-Landing Analysis for the First Lunar Outpost Missions: Apollo Configuration," NASA Report JSC-25895, 1992.

[16]Broome, J.; et.al., "Integrated Entry and Landing Characterization and Sensitivity Study", NASA Johnson Space Center, TDS-04-014, Doc # Flt-Dyn CEV-06-101.

[17]Schneider, W. C.: "Mars TransHab Design Study Team Presentation," Internal Presentation, National Aeronautics and Space Administration, Johnson Space Center, Houston, Texas, 1997.